MATERIALS SCIENCE

A sustainable single-component "Silk nacre"

Zongpu Xu[1]†, Mingrui Wu[1], Weiwei Gao[2], Hao Bai[1]*

Synthetic composite materials constructed by hybridizing multiple components are typically unsustainable due to inadequate recyclability and incomplete degradation. In contrast, biological materials like silk and bamboo assemble pure polymeric components into sophisticated multiscale architectures, achieving both excellent performance and full degradability. Learning from these natural examples of bio-based "single-component" composites will stimulate the development of sustainable materials. Here, we report a single-component "Silk nacre," where nacre's typical "brick-and-mortar" structure has been replicated with silk fibroin only and by a facile procedure combining bidirectional freezing, water vapor annealing, and densification. The biomimetic design endows the Silk nacre with mechanical properties superior to those of homogeneous silk material, as well as to many frequently used polymers. In addition, the Silk nacre shows controllable plasticity and complete biodegradability, representing an alternative substitute to conventional composite materials.

INTRODUCTION

High-performance composite materials are in great demand in many fields, such as building construction, automobile manufacturing, aircraft technology, and biomedical engineering (*1*–*5*). To this end, the strategy of hybridizing multiple components, including metals, ceramics, and polymers, is generally used. Despite the progress achieved in improved performance for such composite materials, concerns over their sustainability increase rapidly (*6*), due to the difficulty of removing individual components for recycling and incomplete degradation. In particular, environmental issues associated with the pollution of waste plastics and synthetic composites have aroused increasing attention worldwide (*7*–*9*). Therefore, constructing more high-performance and sustainable composites from bio-based polymers becomes increasingly vital, where many natural polysaccharides (cellulose, chitin, and starch) or proteins (silk, collagen, and keratin) can serve as promising building blocks (*1*, *6*).

Biological materials usually achieve excellent performance by building sophisticated multiscale architectures, despite their limited selection over components (*10*–*16*). This strategy is particularly evident in pure polymeric materials like silk and bamboo, which are also categorized as "single-component" composite in the sense that they have composite architectures. For example, with pure biopolymer, silk achieves both high strength and toughness by building nanosized crystalline phase embedded in an amorphous matrix (*17*). The same strategy applies to bamboo, where biopolymer matrix is reinforced by hierarchically aligned cellulose fibrils (*11*). Learning from these natural examples will stimulate the development of high-performance and sustainable composite materials. This has become increasingly important as typical synthetic composites are difficult to recycle such as glass fiber–reinforced composites used in wind power blades and tires reinforced with functional nanofillers. Hence, the natural strategy of building high-performance materials by efficient integration of single components into composite architectures represents a more sustainable solution than the typical strategy of hybridizing multiple components. However, the achievement of using this bioinspired strategy is still far from satisfaction in terms of material performances, mainly due to our limited capability of mimicking the sophisticated architectures of biological materials.

Here, as a proof of concept, a silk-based nacre-like composite material, denoted as "Silk nacre," is constructed by using one single component (silk fibroin) as the building block while mimicking natural nacre's composite structure. Generally speaking, nacre is formed by living animals (mostly mollusks) in the natural environment and presents as a composite material, which is reported to consist of about 95 weight % (wt %) aragonite ($CaCO_3$) and ~5 wt % biopolymers (*2*, *15*). The layered aragonite platelets are bonded by a thin layer of biopolymer, forming a brick-and-mortar–like architecture. Nacre's hierarchical structures and the strong interfacial interactions between the inorganic "bricks" and the organic "mortar" endow it with remarkable mechanical properties, combining both high strength and toughness. In contrast to common organic-inorganic nacre-like composites, the bricks and the mortar in the Silk nacre derive from the same component, which are compactly integrated without any other glue. The composite structures of the Silk nacre endow it with mechanical properties superior to those of a homogeneous silk material, with its bending strength, modulus, and strain significantly improved by 67, 37, and 19%, respectively. Moreover, the Silk nacre shows controllable plasticity, which is usually difficult to achieve regarding strong and bulk nacre-like composites. In addition, the Silk nacre is completely biodegradable with the enzyme pronase E at 37°C, indicating its favorable environmental friendliness. We believe that this work paves an effective way to develop high-performance and sustainable materials with a simple component and a facile manufacturing procedure.

RESULTS

Fabrication of the Silk nacre

During the past decades, nacre has drawn considerable attention for its elegant "brick-and-mortar" architecture (*15*, *16*, *18*). Similar to many biological materials, nacre also achieves both high strength and toughness, which are generally mutually exclusive in synthetic composites (*1*, *19*, *20*). To build strong and tough bulk nacre-like materials, a series of procedures, including construction of an ordered nanomaterial framework (*21*–*24*), sintering or densification (*21*, *22*), polymer infiltration, and curing (*23*, *24*), are frequently applied. In this

[1]State Key Laboratory of Chemical Engineering, College of Chemical and Biological Engineering, Zhejiang University, Hangzhou 310027, China. [2]Department of Polymer Science and Engineering, Zhejiang University, Hangzhou 310027, China.
*Corresponding author. Email: hbai@zju.edu.cn
†Present address: Institute of Applied Bioresources, College of Animal Sciences, Zhejiang University, Hangzhou 310058, China.

work, we provided an effective approach to build nacre-like materials, which was simplified both in component types and manufacturing procedures.

The Silk nacre was constructed via bidirectional freezing, water vapor annealing, and densification, as briefly illustrated in Fig. 1 (A to H). First, regenerated silk fibroin solution (10%, w/v) was extracted from silkworm cocoons and then poured into a mold with a polydimethylsiloxane (PDMS) wedge. Because of the low thermal conductivity of PDMS, the ice crystals would start to grow at the bottom end of the wedge when cooling; with both vertical (ΔT_V) and horizontal (ΔT_H) temperature gradients generated by the PDMS wedge, ice crystals grew preferentially vertically away from the cold finger and horizontally along the PDMS wedge at the same time (*25*–*29*). During this process, silk fibroin molecules were expelled from the freezing solution to the space between lamellar ice crystals (Fig. 1, C and D). After the sublimation of ice crystals, a silk aerogel was obtained with a typical long-range aligned lamellar structure (Fig. 1, E and I). Mimicking nacre's architectures, the laminae served as the bricks (Fig. 1J), and their thicknesses could be regulated from ~1 to 4.5 μm by simply changing the cooling temperatures (fig. S1). To further generate the mortar, freeze-dried silk aerogel was put under 75% relative humidity and room temperature for water vapor annealing. In this procedure, water molecules penetrated silk aerogel and plasticized the laminae surfaces (Fig. 1F), leading to improved mobility of silk fibroin chain networks (*30*). Last, the silk aerogel annealed by water vapor was vertically compressed for densification (Fig. 1G; ~10 MPa at room temperature for 20 min), and the Silk nacre was fabricated by adhesion among silk laminae themselves (Fig. 1H). Figure 1K shows the cross section of the Silk nacre, which is similar to that of natural nacre (fig. S2), indicating the compact integration of silk laminae while keeping their aligned lamellar structures. Briefly, a single-component material with nacre-like composite structure was successfully constructed by a facile manufacturing procedure.

Mechanical properties of the Silk nacre

The hierarchical architectures of biological materials play a dominating role regarding to their unrivaled mechanical properties. Presenting as multilayered architectures, the lamina thickness of nacre-like materials is believed to have an effect on their mechanics, depending on the number of interfaces between adjacent laminae (*31*). In this work, the Silk nacre composed of thinner laminae (1 to 2 μm) had higher breaking strength (fig. S3) than thicker laminae (~4.5 μm), due to the abundant interfaces and strong sliding-resistant effect (*31*), with many elongated laminae observed in the fracture surface (fig. S4). On the basis of the above understanding, we selected the Silk nacre with thinner laminae to further investigate the advantages of multilayered structures, and a solvent-casting silk plate with homogeneous structure was prepared for comparison (fig. S5). Although the densities of both materials were around 1.3 g/cm^{-3} and they shared the same component, the Silk nacre and silk plate exhibited

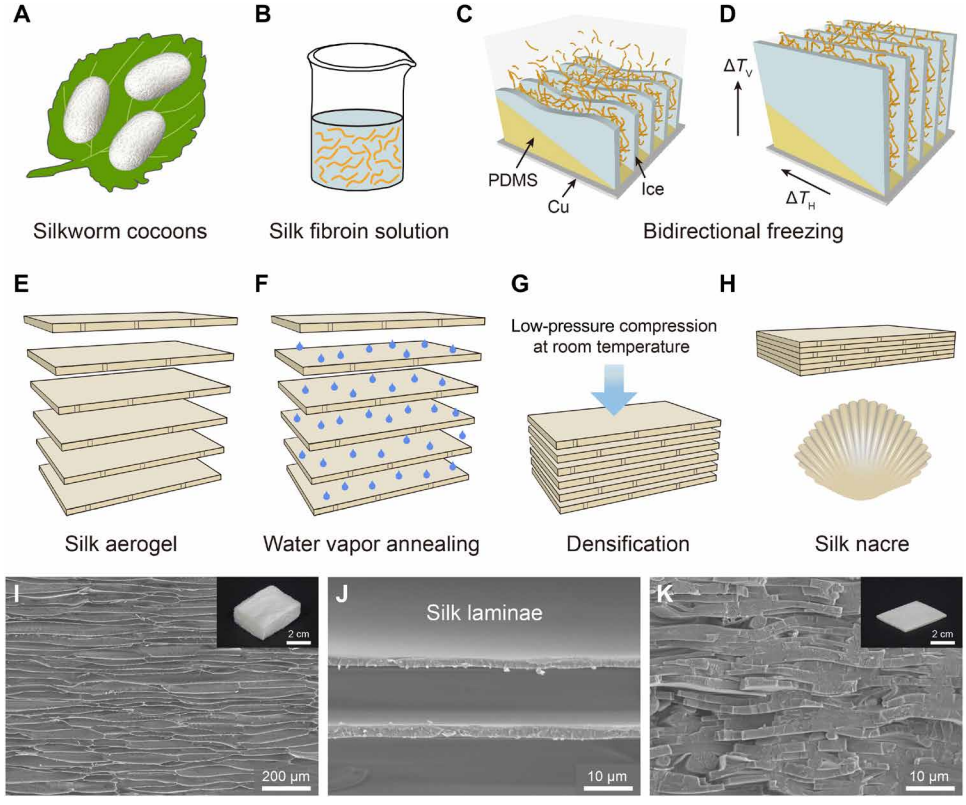

Fig. 1. Schematic diagram of the fabrication processes and the morphology of silk-based single-component nacre-like composite material. (**A** to **D**) Silk fibroin solution is extracted from silkworm cocoons and then undergoes bidirectional freezing process. (**E** to **H**) The as-prepared silk aerogel with lamellar structures is annealed by water vapor at room temperature, then compressed to achieve densification, and lastly presents as the Silk nacre. (**I** and **J**) Scanning electron microscopy (SEM) images of the cross sections of silk aerogel show its long-range aligned lamellar structures (inset is an optical photograph). (**K**) SEM image of the cross section of the Silk nacre shows its nacre-like architectures (inset is an optical photograph).

notably different mechanical performance. As indicated by stress-strain curves of the three-point bending tests, the Silk nacre could withstand higher strength and larger strain (Fig. 2, A and B). It was worth noting that such nacre-like structure simultaneously achieved strengthening and toughing effects; the bending strength, modulus, and strain of the Silk nacre increased to 125 MPa, 6.8 GPa, and 3%, which were 1.67, 1.37, and 1.19 times as high as those of silk plate, respectively. Besides, the strength and modulus of our Silk nacre exceeded many frequently used polymers (Fig. 2C) (*32*–*40*), suggesting its considerable potential as an alternative to synthetic polymers in terms of mechanical performance.

In general, the mechanical properties of silk-based materials are related to the conformation of silk molecules, and previous studies have confirmed that increased crystallinity could improve the breaking strength of silk-based materials (*41*). However, according to Fourier transform infrared (FTIR) spectrum analysis, the content of β sheet in the Silk nacre was much less than that in silk plate (17% versus 36%; Fig. 3, A and B), indicating that the biomimetic structure would lead to better mechanical outcomes beyond the component's intrinsic properties. Figure 3 (C and D) shows the fracture surfaces of silk plate and the Silk nacre, indicating their totally different fracture mechanisms. As a homogeneous material, silk plate exhibited brittle

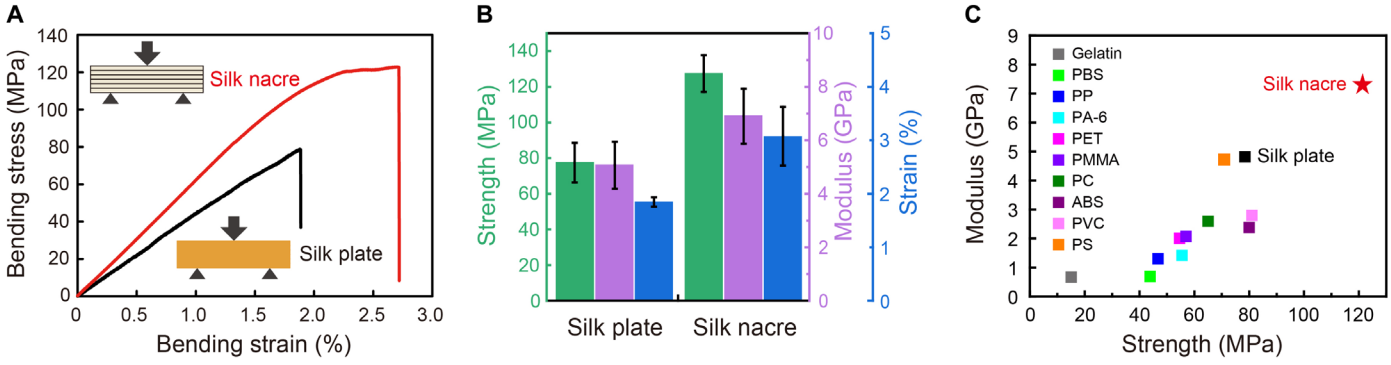

Fig. 2. Comparison of mechanical performance. (**A** and **B**) The Silk nacre shows both better strength and toughness than that of homogeneous silk plate according to the data calculated from stress-strain curves. (**C**) Comparison of modulus and strength among silk plate, the Silk nacre, and various frequently used polymers [from (*32*–*40*)]. PBS, poly(butylene succinate); PP, polypropylene; PA-6, polyamide 6; PET, polyethylene terephthalate; PMMA, polymethyl methacrylate; PC, polycarbonate; ABS, acrylonitrile butadiene styrene; PVC, polyvinyl chloride; PS, polystyrene; the red star refers to the Silk nacre.

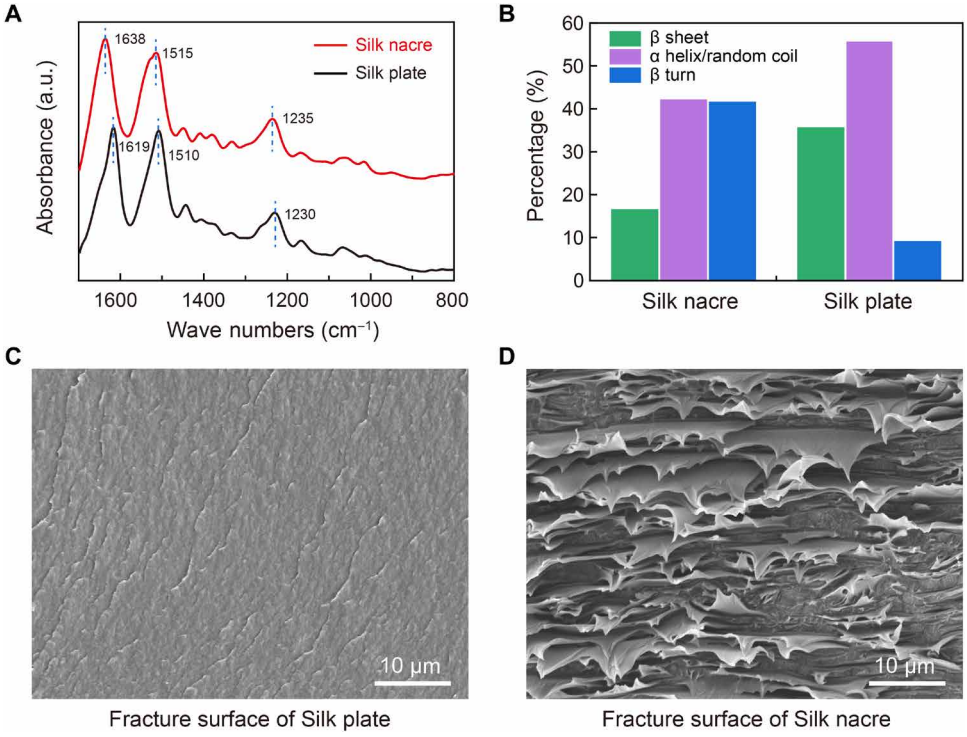

Fig. 3. Comparison of protein conformation and fracture morphology between silk plate and the Silk nacre. (**A** and **B**) Analysis of FTIR spectrum shows lower β sheet content of the Silk nacre than silk plate. a.u., arbitrary units. (**C** and **D**) SEM images of the fracture cross sections indicate totally different fracture mechanisms between silk plate and the Silk nacre.

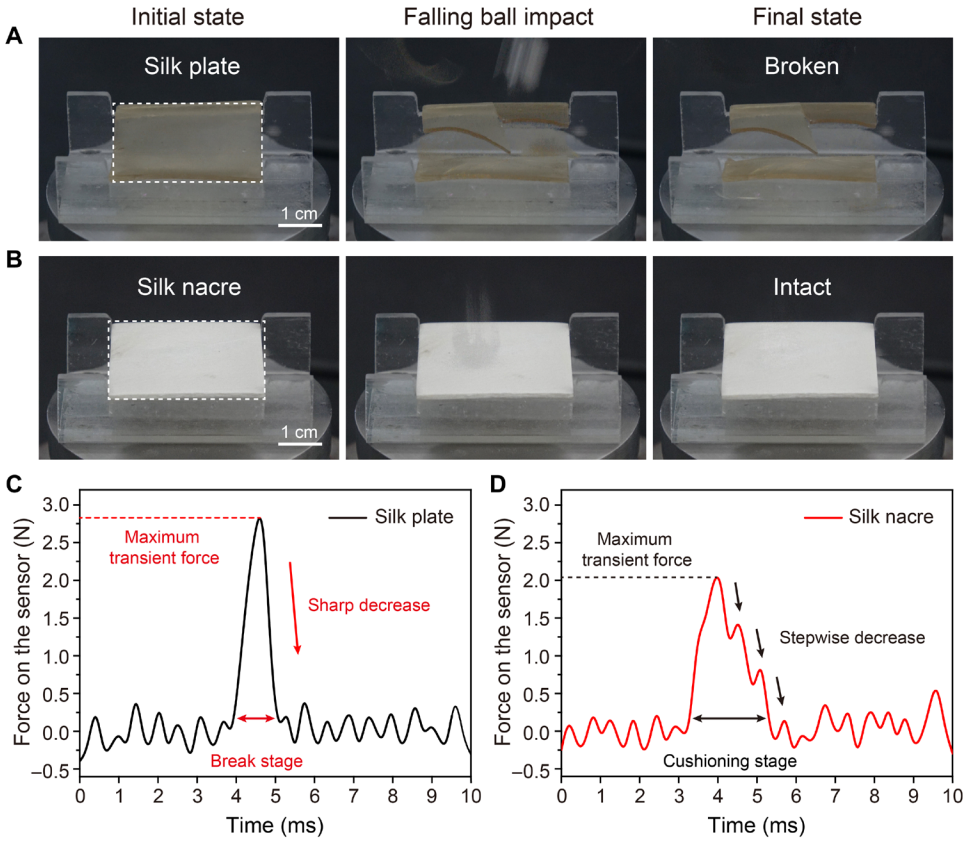

Fig. 4. Comparison of impact resistance between silk plate and the Silk nacre. (**A** and **B**) Typical optical photographs from falling ball impact tests show totally different behaviors of silk plate and the Silk nacre. (**C** and **D**) The force-time curves recorded in the impact tests indicate better impact resistance of the Silk nacre than silk plate in terms of maximum transient force and cushioning effect.

failure and many cracks were observed, resulting in its rapid fracture process. While for the Silk nacre, on one hand, densified interfaces among the bricks and the mortar increased its breaking strength; on the other hand, the lamellar structures and the elongated silk laminae effectively retarded the fracture process. For comparison, another nacre-like silk material was prepared by directly compressing freeze-dried silk aerogel without water vapor annealing. Because of lack of the mortar, such material had relatively loose structure and showed a marked decline in mechanical properties (only 20% of the strength to the Silk nacre; fig. S6), which further demonstrated the importance of building the brick-and-mortar structure. In addition, the pressure applied to the water vapor–annealed silk aerogel also influenced the interactions between the bricks and the mortar. When the pressure is lower than 10 MPa (e.g., 6 or 8 MPa), the breaking strength of obtained silk material decreased significantly (about 35 or 55% of the strength to the Silk nacre; fig. S7A), mainly resulted from the reduction in their structural densification, with interlamellar voids observed at the fracture surfaces (fig. S7, B and C).

We also investigated the impact resistance of the Silk nacre and silk plate via falling ball impact tests (movie S1). As shown in Fig. 4 (A and B), silk plate broke into pieces after falling ball's strike, while the Silk nacre kept intact still, indicating its better impact resistance. The impact force on silk plate and the Silk nacre were recorded by a mechanical sensor, and notable difference was observed in terms of the maximum transient force and cushioning effect (Fig. 4, C and D). For silk plate, the maximum transient force was around 2.8 N, and it suddenly dropped after the contact with the falling ball. In contrast, the value for the Silk nacre was about 2 N, and it decreased in stepwise, suggesting that the lamellar structures endowed the Silk nacre with notable cushioning effect and impact resistance (*42*). Moreover, the results of Split-Hopkinson pressure bar (SHPB) tests at high-strain rate compression (10,000 s^{-1}) further illustrated the better impact resistance of the Silk nacre due to its higher breaking strength and larger deformation strain (fig. S8).

Plasticity and biodegradability of the Silk nacre

Despite high strength and stiffness, the Silk nacre was able to be manufactured into various shapes by a very simple method. Steam could break the hydrogen bonds inside the Silk nacre and made it soft (*30*), which then became flexible enough to be processed into wavy, curved, and helical shapes; after cooling for several minutes in air, the shapes of the Silk nacre were fixed (Fig. 5A). Unlike traditional shaping procedure, where molten or quasi-liquid polymer is put into a certain mold, we provide a quasi-solid and mold-free approach. The processed Silk nacre maintained its intriguing mechanical performance, as it could withstand around 1000 times of its own weight (Fig. 5B). In addition, the Silk nacre showed complete biodegradability due to the intrinsic nature of silk fibroin. As is known, environmental pollution of waste plastics and synthetic composites is becoming increasingly serious worldwide in recently years (*7*–*9*), thus growing attention has been paid to biosourced materials (*6*, *43*, *44*). During the past decade, silk-based materials have been widely studied to partly substitute synthetic polymers,

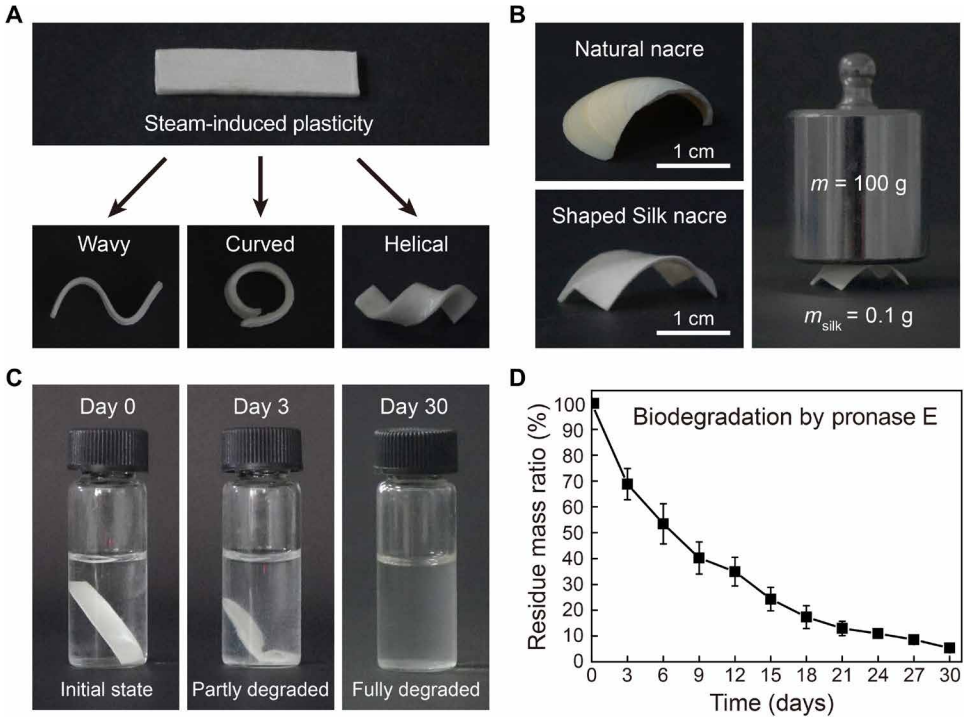

Fig. 5. Plasticity and biodegradability of the Silk nacre. (**A**) The Silk nacre can be manufactured into various complex shapes via steam-induced plasticity. (**B**) The processed Silk nacre can withstand around 1000 times its own weight. (**C**) Optical photographs show the morphological changes at different time points during the degradation period. (**D**) The residue mass-time curve indicates the Silk nacre can be completely biodegraded with the enzyme pronase E within 30 days.

whether as tissue engineering scaffolds, substrates in flexible electronics, or reinforcement elements (*45*–*49*). Figure 5 (C and D) shows the biodegradation process of the Silk nacre and the corresponding variation curve of its residue mass, illustrating that it can be fully biodegraded with the enzyme pronase E at 37°C within 30 days. Hence, such single-component Silk nacre is environment-friendly and sustainable for on-demand disposal and recycle after service life.

DISCUSSION

In summary, we propose and successfully demonstrate a bioinspired strategy to construct high-performance and sustainable composite materials with single polymeric component. Despite its simple composition (pure silk fibroin), our Silk nacre achieves excellent mechanical properties by mimicking nacre's brick-and-mortar structure. Together with its controllable plasticity and complete biodegradability, our Silk nacre suggests a great opportunity to partly substitute conventional composite materials that are increasingly suffering from difficult recycling and incomplete degradation. This work will not only provide an insightful perspective for better understanding the sophisticated multiscale architectures of biological materials but also paves an effective way for the development of high-performance and sustainable composites with a simple component and a facile manufacturing procedure.

MATERIALS AND METHODS

Materials

Bombyx mori silkworm cocoons were purchased from Yiwu Ruiheng Co. Ltd., China. Na_2CO_3, LiBr, and HFIP (1,1,1,3,3,3-hexafluoro-2-propanol) were purchased from Shanghai Sinopharm Group Co. Ltd., China. Pronase E was purchased from Jiangsu Qianye Biotechnology Co. Ltd., China. PDMS (SYLGARD 184) was purchased from Dow Corning Co. Ltd., China. For the preparation of bidirectional freezing molds, acrylic tubes were sealed with a copper plate on one end and tilted to an angle of around 20°. The PDMS precursor was poured into the tube to cover the copper plate, yielding a PDMS wedge after curing at 60°C for 4 hours.

Fabrication of silk plate and the Silk nacre

First, regenerated silk fibroin solution was extracted from silkworm cocoons according to a routine procedure, including degumming, dissolution, dialysis, and concentration processes. Then, silk fibroin solution (10%, w/v) was poured into the bidirectional freezing molds and frozen at various temperatures of cooling stage, including −30° and −90°C via a cryogenic ethanol bath and −196°C via liquid nitrogen. The entirely frozen samples were taken out from the molds and lyophilized for 48 hours under 5 Pa and −80°C by a freeze dryer (Labconco 8811). For the preparation of silk plate, the freeze-dried silk aerogel was first dissolved in HFIP to obtain a 15% (w/v) solution, and then the silk-HFIP solution was poured onto an aluminum dish repeatedly along with the HFIP evaporation. After curing in methanol for 72 hours and drying in an oven at 60°C for 24 hours, silk plate was lastly obtained. For the preparation of the Silk nacre, the freeze-dried silk aerogel was put into a closed hood with 75% relative humidity for water vapor annealing at room temperature and then vertically compressed (~10 MPa) at room temperature for 20 min. In contrast, the Silk nacre with weak interfaces was obtained by directly compressing (~10 MPa) the as-prepared freeze-dried silk aerogel at room temperature for 20 min.

Characterization

The cross sections of silk aerogel and the Silk nacre as well as the fracture surfaces of silk plate and the Silk nacre were observed by scanning electron microscopy (SEM; Hitachi 3500) with a voltage of 5 kV, and the secondary electron images were collected. The mechanical properties of silk plate and the Silk nacre were tested by a universal testing machine (Instron 5944), in a three-point bending mode (samples in 20 mm by 8 mm by 1 mm). The load cell of 1 kN was selected, and the loading speed was set as 0.015 mm/min. FTIR spectroscopy was used to analyze the conformation and crystallinity of the two samples.

For falling ball impact tests, silk plate and the Silk nacre (samples in 35 mm by 35 mm by 1 mm) were fixed on a holder connecting with a mechanical sensor. A stainless-steel ball (~4 g) freely fell at the height of 100 cm and struck on the samples. The impact process was recorded by a digital camera, and the force-time curve was analyzed from the collected data. For the SHPB tests, the samples were in cylindrical shape (7 mm in diameter and 2 mm in height), and the compression strain rate was set as 10,000 s^{-1}.

Plasticity and biodegradability of the Silk nacre

The Silk nacre was put in steam until it became soft, and then it was processed into different shapes. After taking away from the steam and cooling for a while, the shape of the Silk nacre was fixed. The biodegradation of the Silk nacre was tested by immerging it into 0.01 M phosphate-buffered saline solution containing pronase E (10 U/ml) at 37°C. The residue mass of the Silk nacre was weighed at certain time intervals, and optical photographs were taken to observe its morphology changes.

SUPPLEMENTARY MATERIALS

Supplementary material for this article is available at https://science.org/doi/10.1126/sciadv.abo0946

REFERENCES AND NOTES

1. U. G. Wegst, H. Bai, E. Saiz, A. P. Tomsia, R. O. Ritchie, Bioinspired structural materials. *Nat. Mater.* **14**, 23–36 (2015).
2. L. Mao, H. Gao, H. Yao, L. Liu, H. Colfen, G. Liu, S. Chen, S. Li, Y. Yan, Y. Liu, S. Yu, Synthetic nacre by predesigned matrix-directed mineralization. *Science* **354**, 107–110 (2016).
3. Q. Guan, H. Yang, Z. Han, Z. Ling, S. Yu, An all-natural bioinspired structural material for plastic replacement. *Nat. Commun.* **11**, 5401 (2020).
4. S. Deville, E. Saiz, R. K. Nalla, A. P. Tomsia, Freezing as a path to build complex composites. *Science* **311**, 515–518 (2006).
5. A. R. Studart, Towards high-performance bioinspired composites. *Adv. Mater.* **24**, 5024–5044 (2012).
6. A. K. Mohanty, S. Vivekanandhan, J. M. Pin, M. Misra, Composites from renewable and sustainable resources: Challenges and innovations. *Science* **362**, 536–542 (2018).
7. J. R. Jambeck, R. Geyer, C. Wilcox, T. R. Siegler, M. Perryman, A. Andrady, R. Narayan, K. L. Law, Plastic waste inputs from land into the ocean. *Science* **347**, 768–771 (2015).
8. R. Geyer, J. R. Jambeck, K. L. Law, Production, use, and fate of all plastics ever made. *Sci. Adv.* **3**, e1700782 (2017).
9. J. Smith, S. Vignieri, A devil's bargain. *Science* **373**, 34–35 (2021).
10. M. Eder, S. Amini, P. Fratzl, Biological composites-complex structures for functional diversity. *Science* **362**, 543–547 (2018).
11. M. K. Habibi, A. T. Samaei, B. Gheshlaghi, J. Lu, Y. Lu, Asymmetric flexural behavior from bamboo's functionally graded hierarchical structure: Underlying mechanisms. *Acta Biomater.* **16**, 178–186 (2015).
12. F. Barthelat, Z. Yin, M. J. Buehler, Structure and mechanics of interfaces in biological materials. *Nat. Rev. Mater.* **1**, 16007 (2016).
13. M. A. Meyers, J. McKittrick, P.-Y. Chen, Structural biological materials: Critical mechanics-materials connections. *Science* **339**, 773–779 (2013).
14. F. G. Omenetto, D. L. Kaplan, New opportunities for an ancient material. *Science* **329**, 528–531 (2010).
15. J. Gim, N. Schnitzer, L. M. Otter, Y. Cui, S. Motreuil, F. Marin, S. E. Wolf, D. E. Jacob, A. Misra, R. Hovden, Nanoscale deformation mechanics reveal resilience in nacre of *Pinna nobilis* shell. *Nat. Commun.* **10**, 4822 (2019).
16. J. Gim, A. Koch, L. M. Otter, B. H. Savitzky, S. Erland, L. A. Estroff, D. E. Jacob, R. Hovden, The mesoscale order of nacreous pearls. *P. Natl. Acad. Sci. U.S.A.* **118**, e2107477118 (2021).
17. S. Ling, D. L. Kaplan, M. J. Buehler, Nanofibrils in nature and materials engineering. *Nat. Rev. Mater.* **3**, 18016 (2018).
18. R. Hovden, S. E. Wolf, M. E. Holtz, F. Marin, D. A. Muller, L. A. Estroff, Nanoscale assembly processes revealed in the nacroprismatic transition zone of *Pinna nobilis* mollusc shells. *Nat. Commun.* **6**, 10097 (2015).
19. E. M. Gerhard, W. Wang, C. Li, J. Guo, I. T. Ozbolat, K. M. Rahn, A. D. Armstrong, J. Xia, G. Qian, J. Yang, Design strategies and applications of nacre-based biomaterials. *Acta Biomater.* **54**, 21–34 (2017).
20. Q. Cheng, C. Huang, A. P. Tomsia, Freeze casting for assembling bioinspired structural materials. *Adv. Mater.* **29**, 1703155 (2017).
21. H. Bai, F. Walsh, B. Gludovatz, B. Delattre, C. Huang, Y. Chen, A. P. Tomsia, R. O. Ritchie, Bioinspired hydroxyapatite/poly(methyl methacrylate) composite with a nacre-mimetic architecture by a bidirectional freezing method. *Adv. Mater.* **28**, 50–56 (2016).
22. N. Zhao, M. Li, H. Gong, H. Bai, Controlling ice formation on gradient wettability surface for high-performance bioinspired materials. *Sci. Adv.* **6**, eabb4712 (2020).
23. G. Du, A. Mao, J. Yu, J. Hou, N. Zhao, J. Han, Q. Zhao, W. Gao, T. Xie, H. Bai, Nacre-mimetic composite with intrinsic self-healing and shape-programming capability. *Nat. Commun.* **10**, 800 (2019).
24. J. Han, G. Du, W. Gao, H. Bai, An anisotropically high thermal conductive boron nitride/epoxy composite based on nacre-mimetic 3D network. *Adv. Funct. Mater.* **29**, 1900412 (2019).
25. H. Bai, Y. Chen, B. Delattre, A. P. Tomsia, R. O. Ritchie, Bioinspired large-scale aligned porous materials assembled with dual temperature gradients. *Sci. Adv.* **1**, e1500849 (2015).
26. N. Zhao, M. Yang, Q. Zhao, W. Gao, T. Xie, H. Bai, Superstretchable nacre-mimetic graphene/poly(vinyl alcohol) composite film based on interfacial architectural engineering. *ACS Nano* **11**, 4777–4784 (2017).
27. M. Yang, N. Zhao, Y. Cui, W. Gao, Q. Zhao, C. Gao, H. Bai, T. Xie, Biomimetic architectured graphene aerogel with exceptional strength and resilience. *ACS Nano* **11**, 6817–6824 (2017).
28. D. Li, X. Bu, Z. Xu, Y. Luo, H. Bai, Bioinspired multifunctional cellular plastics with a negative Poisson's ratio for high energy dissipation. *Adv. Mater.* **32**, e2001222 (2020).
29. Y. Cui, Y. Wang, Z. Shao, A. Mao, W. Gao, H. Bai, Smart sponge for fast liquid absorption and thermal responsive self-squeezing. *Adv. Mater.* **32**, e1908249 (2020).
30. X. Hu, K. Shmelev, L. Sun, E. Gil, S. Park, P. Cebe, D. L. Kaplan, Regulation of silk material structure by temperature-controlled water vapor annealing. *Biomacromolecules* **12**, 1686–1696 (2011).
31. H.-L. Gao, S.-M. Chen, L.-B. Mao, Z.-Q. Song, H.-B. Yao, H. Cölfen, X.-S. Luo, F. Zhang, Z. Pan, Y.-F. Meng, Y. Ni, S.-H. Yu, Mass production of bulk artificial nacre with excellent mechanical properties. *Nat. Commun.* **8**, 287 (2017).
32. V. Zal, H. Moslemi Naeini, A. R. Bahramian, A. H. Behravesh, B. Abbaszadeh, Investigation and analysis of glass fabric/PVC composite laminates processing parameters. *Sci. Eng. Compos. Mater.* **25**, 529–540 (2018).
33. B. P. Singh, A. Babal, J. Jyoti, S. Sharma, A. Arya, S. R. Dhakate, Synergistic effect on static and dynamic mechanical properties of carbon fiber-multiwalled carbon nanotube hybrid polycarbonate composites. *RSC Adv.* **6**, 67954–67967 (2016).
34. M. Naderzadeh, M. R. Monazzam, I. Ghasemi, H. Arabalibeik, Investigation on sound absorption function and mechanical behavior of polycarbonate/nanosilica-based nanocomposites. *Polym-Plast. Technol.* **57**, 387–393 (2017).
35. R. H. Pour, A. Hassan, M. Soheilmoghaddam, H. C. Bidsorkhi, Mechanical, thermal, and morphological properties of graphene reinforced polycarbonate/acrylonitrile butadiene styrene nanocomposites. *Polym. Compos.* **37**, 1633–1640 (2016).
36. S. Kumar, R. Singh, T. P. Singh, A. Batish, On flexural and pull out properties of 3D printed PLA based hybrid composite matrix. *Mater. Res. Express* **7**, 015330 (2020).
37. C. Wu, W. Lai, C. Wang, Effects of surface modification on the mechanical properties of flax/beta-polypropylene composites. *Materials* **9**, 314 (2016).
38. Y. Hamid, A. A. Bakar, N. Deirram, Mechanical and morphological properties of wasteEurycoma longifoliafiber/montmorillonite reinforced poly(vinyl chloride) hybrid composites. *J. Appl. Polym. Sci.* **128**, 1170–1175 (2013).
39. J. G. Jeon, H. C. Kim, J. Kim, T. J. Kang, Polystyrene nanocomposites reinforced with phenyl isocyanate-treated cellulose nanofibers. *Funct. Compos. Struct.* **2**, 015002 (2020).
40. T. J. Quill, M. K. Smith, T. Zhou, M. G. S. Baioumy, J. P. Berenguer, B. A. Cola, K. Kalaitzidou, T. L. Bougher, Thermal and mechanical properties of 3D printed boron nitride-ABS composites. *Appl. Compos. Mater.* **25**, 1205–1217 (2017).

41. C. Guo, C. Li, H. V. Vu, P. Hanna, A. Lechtig, Y. Qiu, X. Mu, S. Ling, A. Nazarian, S. J. Lin, D. L. Kaplan, Thermoplastic moulding of regenerated silk. *Nat. Mater.* **19**, 102–108 (2020).
42. Q. Guan, H. Yang, Z. Han, L. Zhou, Y. Zhu, Z. Ling, H. Jiang, P. Wang, T. Ma, H. Wu, S. Yu, Lightweight, tough, and sustainable cellulose nanofiber-derived bulk structural materials with low thermal expansion coefficient. *Sci. Adv.* **6**, eaaz1114 (2020).
43. A. Bourmaud, J. Beaugrand, D. U. Shah, V. Placet, C. Baley, Towards the design of high-performance plant fibre composites. *Prog. Mater. Sci.* **97**, 347–408 (2018).
44. S. Ling, W. Chen, Y. Fan, K. Zheng, K. Jin, H. Yu, M. J. Buehler, D. L. Kaplan, Biopolymer nanofibrils: Structure, modeling, preparation, and applications. *Prog. Polym. Sci.* **85**, 1–56 (2018).
45. B. B. Mandal, A. Grinberg, E. S. Gil, B. Panilaitis, D. L. Kaplan, High-strength silk protein scaffolds for bone repair. *P. Natl. Acad. Sci. U.S.A.* **109**, 7699–7704 (2012).
46. Z. Xu, L. Shi, M. Yang, H. Zhang, L. Zhu, Fabrication of a novel blended membrane with chitosan and silk microfibers for wound healing: Characterization, in vitro and in vivo studies. *J. Mater. Chem. B* **3**, 3634–3642 (2015).
47. J. Melke, S. Midha, S. Ghosh, K. Ito, S. Hofmann, Silk fibroin as biomaterial for bone tissue engineering. *Acta Biomater.* **31**, 1–16 (2016).
48. K. Yang, J. Guan, K. Numata, C. Wu, S. Wu, Z. Shao, R. O. Ritchie, Integrating tough Antheraea pernyi silk and strong carbon fibres for impact-critical structural composites. *Nat. Commun.* **10**, 3786 (2019).
49. Z. Xu, M. Wu, W. Gao, H. Bai, A transparent, skin-inspired composite film with outstanding tear resistance based on flat silk cocoon. *Adv. Mater.* **32**, e2002695 (2020).

Acknowledgments: We are grateful to H. Gao from University of Science and Technology of China for help with experiments on SHPB tests. **Funding:** This work was supported by the National Natural Science Foundation of China (grant nos. 22075244, 51722306, and 21674098), Shanxi-Zheda Institute of Advanced Materials and Chemical Engineering (grant 2021SZ-TD009), National Key Research and Development Program of China (grant 2017YFC1103900), and State Key Laboratory of Chemical Engineering (grant SKL-ChE-20 T06). **Author contributions:** H.B. conceived the concept and supervised the project. Z.X. and M.W. performed the experiments. Experimental results were analyzed through contributions of all authors. H.B., Z.X., and W.G. wrote the manuscript. **Competing interests:** The authors declare that they have no competing interests. **Data and materials availability:** All data needed to evaluate the conclusions in the paper are present in the paper and/or the Supplementary Materials.

Submitted 17 January 2022
Accepted 29 March 2022
Published 13 May 2022
10.1126/sciadv.abo0946